

Incipient plasticity in 4H-SiC during quasistatic nanoindentation

Saurav Goel^{ab*}, Jiwang Yan^b, Xichun Luo^c and Anupam Agrawal^d

^a School of Mechanical and Aerospace Engineering, Queen's University, Belfast, BT95AH, UK

^b Department of Mechanical Engineering, Keio University, Yokohama, 223-8522, Japan

^c Department of Design, Manufacture and Engineering Management, University of Strathclyde, Glasgow, G11XQ, UK

^d Department of Business Administration, University of Illinois at Urbana Champaign, 61820, USA

*Corresponding author Tel.: +44-028-90975625, Email address: s.goel@qub.ac.uk, Fax: +44-028-90974148

Abstract:

Silicon carbide (SiC) is an important orthopaedic material due to its inert nature and superior mechanical and tribological properties. Some of the potential applications of silicon carbide include coating for stents to enhance hemocompatibility, coating for prosthetic-bearing surfaces and uncemented joint prosthetics. This study is the first to explore nanomechanical response of single crystal 4H-SiC through quasistatic nanoindentation. Displacement controlled quasistatic nanoindentation experiments were performed on single crystal 4H-SiC specimen using a blunt Berkovich indenter (300 nm tip radius) at extremely fine indentation depths of 5 nm, 10 nm, 12 nm, 20 nm, 25 nm and 50 nm. Load-displacement curve obtained from the indentation experiments showed yielding or incipient plasticity in 4H-SiC typically at a shear stress of about 21 GPa (~ an indentation depth of 33.8 nm) through a pop-in event. An interesting observation was that the residual depth of indent showed three distinct patterns: (i) Positive depth hysteresis above 33 nm, (ii) no depth hysteresis at 12 nm, and (iii) negative depth hysteresis below 12 nm. This contrasting depth hysteresis phenomenon is hypothesized to originate due to the existence of compressive residual stresses (upto 143 MPa) induced in the specimen by the polishing process prior to the nanoindentation.

Keywords: SiC; nanoindentation, plasticity, elastic response

1. Introduction

Silicon carbide (SiC) is an extremely hard and brittle non-oxide ceramic material. It has been demonstrated that, due to its superior properties, such as chemical inertness, high thermal conductivity, high carrier saturation velocity, high specific stiffness (E/ρ) and high-temperature resistance, SiC is an appropriate choice to replace silicon for advanced ultra precision engineering applications especially in the electronic industry [1]. SiC is also recognized as a potential candidate for quantum computing applications as a substitute for diamond [2], in space-based laser mirrors [3] and for the development of thermal protection system (TPS) materials for defence applications [4]. Demand of SiC is growing further in weapons, aerospace, microelectronic and bio-medical applications as well as in “big-science” programmes such as the European Extremely Large Telescope (E-ELT), the Atacama Large Millimeter / submillimeter Array (ALMA) and next generation extreme ultraviolet (EUV) lithography steppers.

SiC is also finding amazing applications in bio-medical sector especially as being a semi-conductor material because of being more bio-compatible over silicon [5]. Traditional orthopaedic materials such as cobalt chrome (CoCr), stainless steel and titanium on account of being low wear and oxidation resistant, succumb to bone loss which causes implant loosening resulting in a reactive implant surface while SiC is capable of permanently integrating into the new bone growth on account of low wear debris and metallosis and is thus very effective as coating for stents to enhance hemocompatibility and as a coating for prosthetic-bearing surfaces and uncemented joint prosthetics [6]. Nanocrystalline silicon carbide (SiC) is therefore known to carry the potential to become an important and an interface biomaterial which will connect the three disparate disciplines of electronics, material science and biological world [7]. Field results of Kalnsis *et al.* [8] applied directly on various patients provide further support for the above arguments: they found that amorphous silicon carbide stents are more effective than stainless steel in reducing the early and late coronary events.

Mechanical processing of SiC in particular is a daunting task at the moment owing primarily to the following unique characteristics of SiC [9-10]:

1. SiC exhibits low thermal coefficient and high thermal conductivity. This is because of the higher proportion of covalent bonding compared to ionic bonding in SiC (9:1) with the nature of bonding dependent on the Goldschmidt number. The higher proportion of covalent bonding in SiC makes it relatively insensitive to elevated temperature deformation and thus SiC cannot easily be deformed even at elevated temperatures.
2. The ratio of Young's modulus and Vickers hardness in SiC is only about 20 which signify that SiC is highly brittle. This is in contrast to soft ductile materials where this ratio could be as high as 250.
3. The ratio of tensile strength to shear strength in SiC is extremely low (~ 1.5) in contrast to soft ductile metals where this ratio is as high as 10, making them easier to deform through plastic deformation rather than brittle fracture.
4. Low density and low mobility of dislocations leads to high hardness in SiC, while low surface energy due to small density of electrons and high Young's modulus are the reasons of extreme brittleness in SiC. Owing to low surface energy and high Young's modulus, SiC exhibits low fracture toughness and thus poor machinability.
5. To induce the plastic deformation in a ceramic material such as SiC, it requires five independent slip systems to meet the von Mises criterion otherwise twinning or fracture prevails.

Furthermore, SiC exhibits one-dimensional polymorphism: all polytypes have the same tetrahedral arrangement of Si and C atoms but different stacking sequences. It is due to this reason that almost 250 polytypes of silicon carbide (SiC) have been recognized to date [11]. Across all other polytypes, two major polymorphs are α -SiC and β -SiC with hexagonal and zinc-blende lattice structures, respectively. The main engineering properties of β -SiC (3C-SiC) and α -SiC (6H-SiC and 4H-SiC) have already been summarized elsewhere [12].

In the past, experimental trials have been reported on polycrystalline 3C-SiC (CVD-SiC) [13-14], single crystal 6H-SiC [15-17], polycrystalline 6H-SiC (reaction bonded SiC) [18] and single crystal 4H-SiC [19-20]. These studies were focussed on exploring the ductile-regime machining of SiC and have shown that single crystal 6H-SiC exhibits a ductile to brittle transition (DBT) depth of only 70 nm [21] whereas DBT depth in CVD 3C-SiC (polycrystalline) was found to be 550 nm [22]. Compared to these two types of SiC, single crystal 4H-SiC showed a much higher DBT depth of up to 820 nm [20]. Besides offering a larger DBT depth, 4H-SiC also offers the best machined surface and sub-surface integrity [12] across all other major polytypes of SiC which means that it is possible to obtain higher manufacturing productivity for single crystal 4H-SiC. Hence, an investigation on the nanomechanical response of 4H-SiC is scientifically important at this point of time in order to aid cost effective manufacturing of 4H-SiC. State-of-the-art veritable resolution using *in-situ* and *ex-situ* imaging, quasistatic nanoindentation, acoustic emission detection, and high-temperature testing are providing newer insights into nanoscale mechanics of materials. Quasistatic nanoindentation in particular permits systematic examination to enable better understanding of deformation mechanisms, evaluation of mechanical properties, and aspects of plasticity of brittle materials such as SiC. Furthermore, the onset of plastic deformation in a specimen can be studied from such a test merely by a careful assessment of the Load-displacement (P-h) profile. In particular, although pop-in event in the P-h curve may arise due to several reasons depending on the type of specimen e.g. discrete strain accommodation mechanism in metals, formation of cracks in brittle materials or formation of shear bands in metallic glasses [23], but the first pop-in event in this study was observed to be associated with the elastic-plastic transition, signifying plastic deformation of the material.

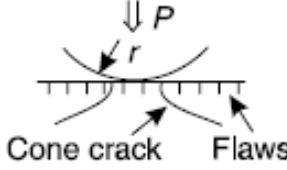
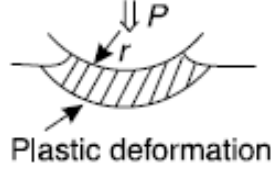
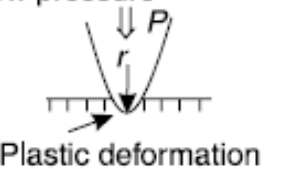
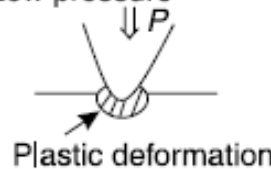
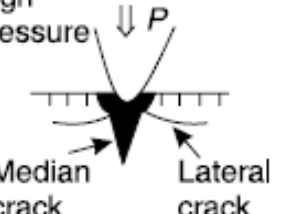
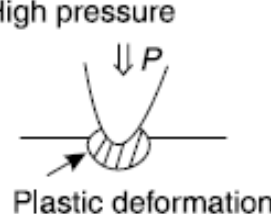
	Brittle materials	Ductile materials
Large radius of tip	 <p>Cone crack Flaws</p>	 <p>Plastic deformation</p>
Small radius of tip	<p>Low pressure</p>  <p>Plastic deformation</p>	<p>Low pressure</p>  <p>Plastic deformation</p>
	<p>High pressure</p>  <p>Median crack Lateral crack</p>	<p>High pressure</p>  <p>Plastic deformation</p>

Figure 1 : Differences in the response of ductile and brittle materials during nanoindentation [24]

Figure 1 show schematically how brittle materials behave differently from ductile materials when they are indented either by a large tipped radii or a small tipped radii indenter. It shows that ductile materials show plastic deformation as the dominant mode of deformation whereas the response of brittle materials is dependent on both the tip radii of the indenter and the magnitude of the load (force applied to the indenter). When brittle materials are indented with a sharp tip, they show plastic deformation at sufficiently low indentation loads, beyond which median and lateral cracks appear [25-26]. The qualitative identification of the elastic-plastic response of brittle materials during their nanoindentation reveal that almost any material, including super-hard substances like diamond and SiC, can be deformed plastically even at low temperatures [27] under the influence of large hydrostatic stresses. With smaller indentation depths, the size of the resulting critical stress field is small enough to avoid cleavage initiated at the defects, but, with larger indentation depths, the larger critical stress field allows for sufficient nuclei for crack propagation, which initiate from defects within the material. These factors motivated the current study, wherein quasistatic nanoindentation experiments were conducted on 4H-SiC to study the incipient plasticity from the force-displacement (P-h) curve.

2. Experimental Details

The nanoindentation tests were performed on a TI 900 Hysitron TriboIndenter which takes advantage of an acoustic and thermal enclosure that enables capturing precise and sensitive readings [28]. Also, its patented capacitive transducer provides superior sensitivity and stability over other similar instruments. The specimen used was a single crystal 4H-SiC wafer having crystal orientation (001), diameter 50 mm and thickness 5 mm which was supplied by PAM-Xiamen Power-way Advanced Material Co. Ltd, China.

The indentation experiments were performed with a three-sided pyramidal Berkovich probe. Of particular relevance in this regard was the nature of the tip apex, which is never atomically sharp and exhibits significant blunting, as measured and verified during the experiments. The method used for the measurement of tip radius involves indenting the tool profile on the copper block. The profile curvature of indentation is copied, fitted to a circle and radius of the circle can be found by simple mathematical analysis [29]. The measurement revealed the tip radius to be about 300 nm. In the experimental context of the current study, the blunting of the Berkovich tip turned out to be a benefit rather than an experimental difficulty. This is because the blunted geometry of the nanoindenter can often be approximated as spherical [30]. With this approximation of the tip geometry, it becomes possible to predict the elastic response using the Hertzian law for mechanical contacts, based on isotropic continuum elasticity. This law predicts a simple power-law form for the elastic portion of the load-displacement curve, $P \propto h^{3/2}$, [31] with a proportionality constant that is fully specified by the radius of the blunted indenter tip and the elastic properties of the two contacting materials. The same is evident from the loading curves as shown later.

Based on the above description, a series of displacement controlled quasistatic nanoindentations were performed at different indentation depths. The displacement control feedback system was preferred over load controlled feedback system to limit the total indentation depth so as to avoid specimen effect [32]. The time allowed for reaching maximum displacement in all the cases was 10 seconds and the indenter was retracted immediately after attaining the peak indentation depth in

duration of 10 seconds. Each test was performed twice (both results were observed to be consistent and hence results for only one set of experiments are presented for brevity). The indents were made following the “quick approach” method. The Quick Approach method moves the indenter tip towards the specimen to sense the exact height of the specimen at a specific point. This move helps in updating the sample safety height with an exact value. Bypassing this step could result in either crashing of the tip into the specimen or would otherwise take several hours to contact the surface. Thus, quick approach method not only helps in ensuring the measurement accuracy at finer depths of indentation, but also ensures that the tip is operated within the “sample safety zones” in that the indenter tip is considered to be safe to avoid any sudden lateral impact load on it. Table 1 shows the various indentation depths used for the experiments. Along with the indentation depth, the table also shows the peak indentation load recorded from the plots obtained from the device and the hysteresis observed in the plots (These are discussed subsequently).

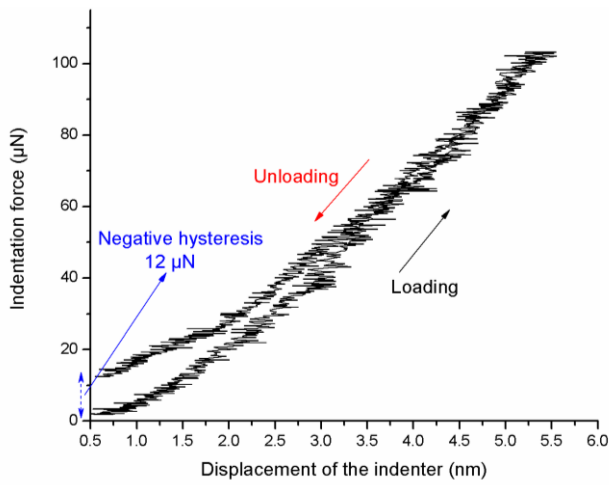
Table 1: Displacement controlled quasistatic nanoindentation experiments performed on 4H-SiC

Experiment Number	Indenter displacement (h) nm	Peak load (P) μN	Hysteresis observed
1	5	103	Negative hysteresis
2	10	275	Negative hysteresis
3	12	300	Complete elastic response with no hysteresis
4	25	825	Elastic response with positive hysteresis
5	30	1265	Elastic response with positive hysteresis
6	50	2425	Elastic + Plastic response

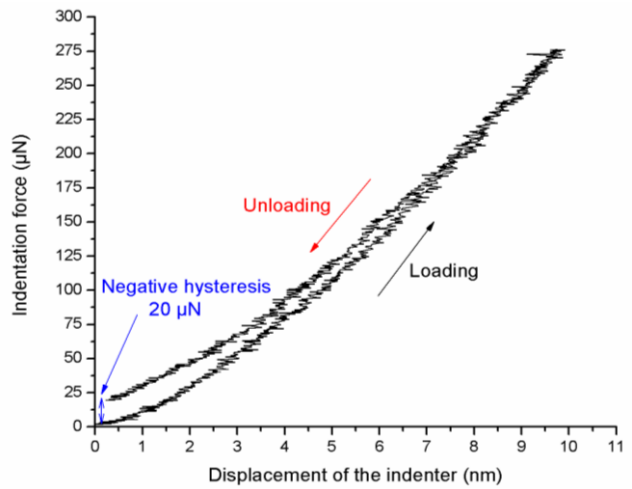
3.0 Results and Discussions

3.1. Depth hysteresis during nanoindentation

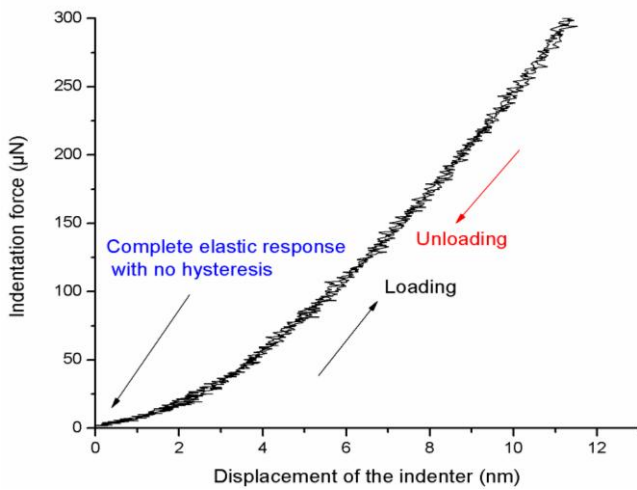
The P-h plots for various depths of indentation performed of 4H-SiC are shown in figure 2. Figures 2(a) and 2(b) show the P-h plots for the indentation depths of 5 nm and 10 nm respectively.



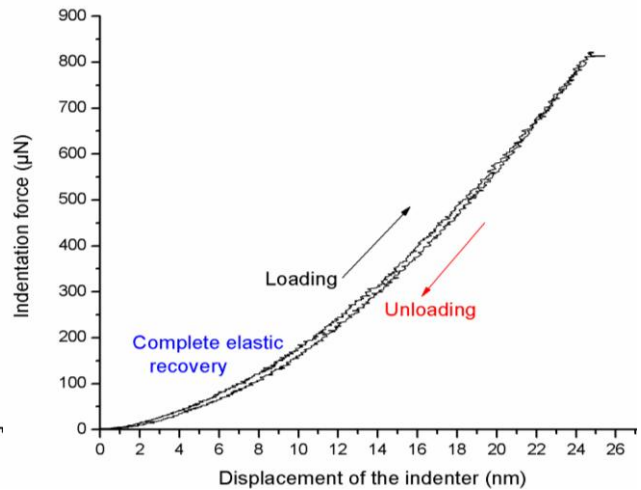
(a) Indentation depth 5 nm



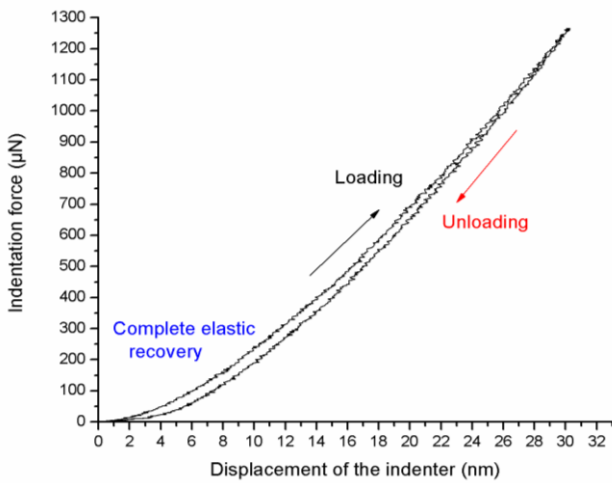
(b) Indentation depth 10 nm



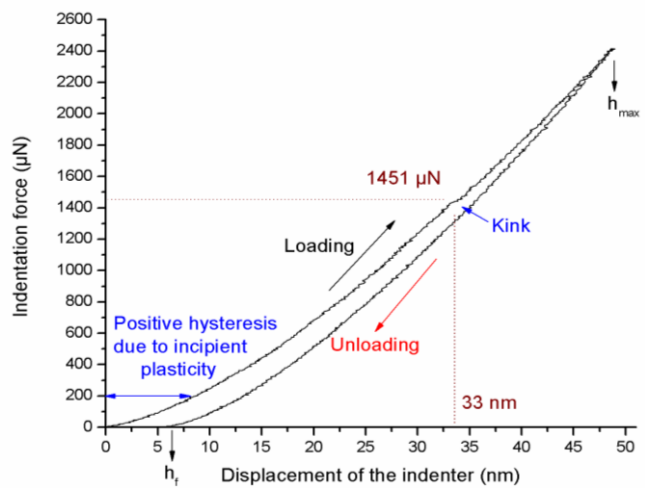
(c) Indentation depth 12 nm



(d) Indentation depth 25 nm



(e) Indentation depth 30 nm



(f) Indentation depth 50 nm

Figure 2: P-h plots for indentations made on single crystal 4H-SiC at various depths

In both the cases (figure 2a and 2b), a negative depth hysteresis of 12 μN and 20 μN respectively can be observed from these plots. Consequently, at these indentation depths, the Oliver and Pharr method to evaluate the material properties from P-h curve cannot be used. Figure 3 shows the AFM imaging and the cross section of the area in case where negative depth hysteresis was observed.

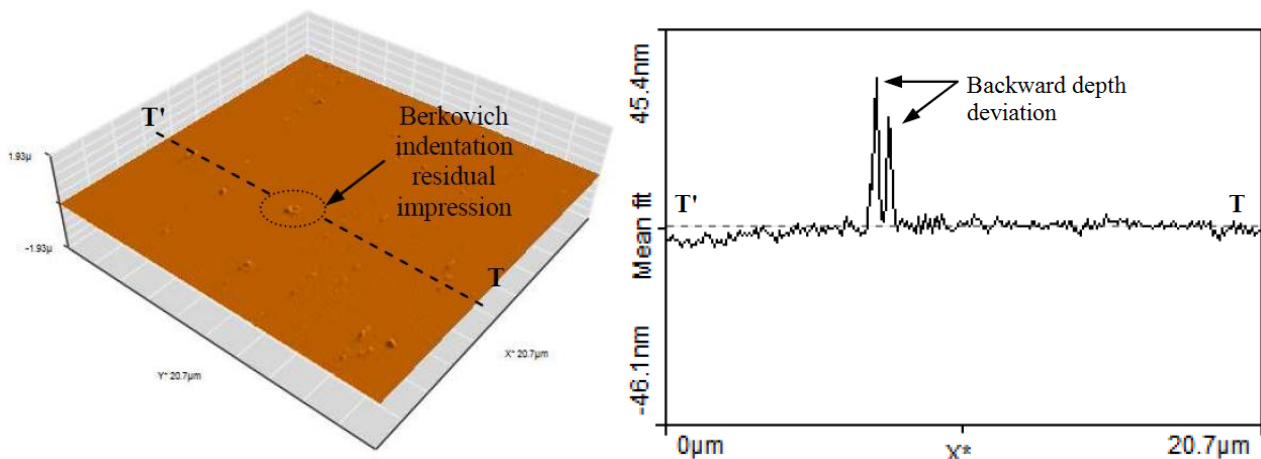
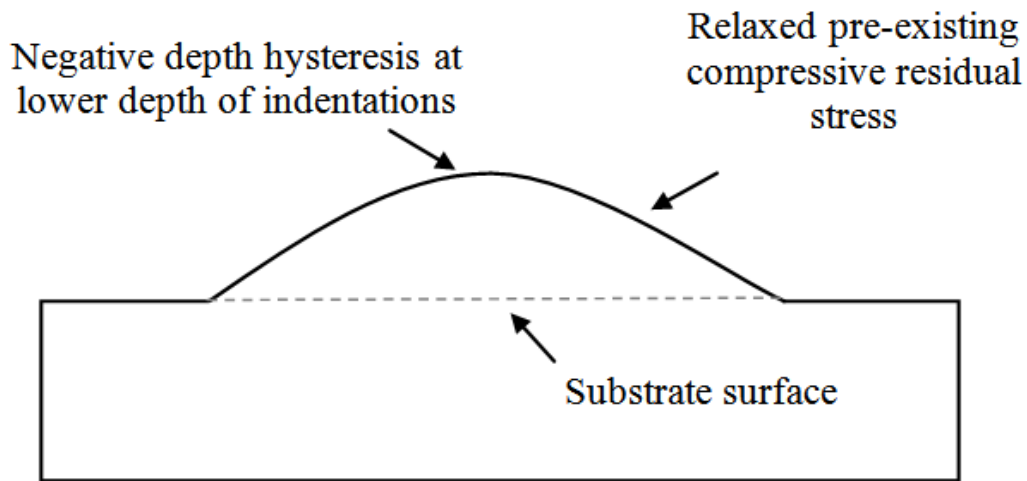


Figure 3: AFM imaging and cross section view of the 4H-SiC specimen highlighting the negative depth hysteresis

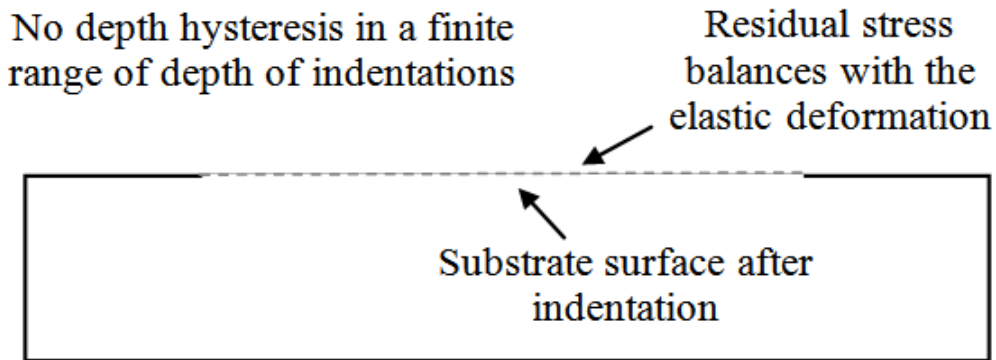
In Figure 3, it may be seen that at sufficiently lower depth of indentation, the surface of the 4H-SiC specimen is projecting upwards (negative depth deviation) after the retraction of the indenter. This is somewhat unusual because extant research on nanoindentation has reported that the unloading curve lags the loading curve and that's why the cross section of the indentation zone shows positive depth deviation. It was not immediately clear as to why this negative depth hysteresis was observed. One thing which may be noted here is that the manufacturer stated that the specimen of 4H-SiC supplied (used in this experimental study) were processed using chemo-mechanical polishing process (CMP). The presence of residual stresses on the polished surface was thus expected to be present. In order to quantify such residual stresses, Raman spectroscopy was performed. Noticeably, against a regular Raman peak of 776 cm^{-1} [33] in 4H-SiC, the experiments showed the Raman peak at about 779.29 cm^{-1} . This reveals the extent of compressive residual stresses in the 4H-SiC specimen to be about 143 MPa (compressive).

Based on this information, it is proposed that the negative depth hysteresis in the unloading force could be due to the annealing and consequent thermal expansion of the surface layer of the specimen. This could happen due to the local heating (high heat at the interface of the indenter and the specimen due to friction) of the surface layer which helps in relieving the compressive residual stresses that are induced in the specimen due to the polishing process carried out on the specimen prior to the nanoindentation process. While compressive residual stresses get relieved due to annealing, the material expands which might have caused an opposite force on the indenter leading to this negative depth hysteresis. This phenomenon implies and aligns with the concept of backward depth deviation which appears in the form of hogging as has been recently observed in the thin films of Diamond like carbon (DLC) [34] and SiC [35]. This implication is also supported from the AFM imaging shown in figure 3 which confirms the presence of negative depth deviation.

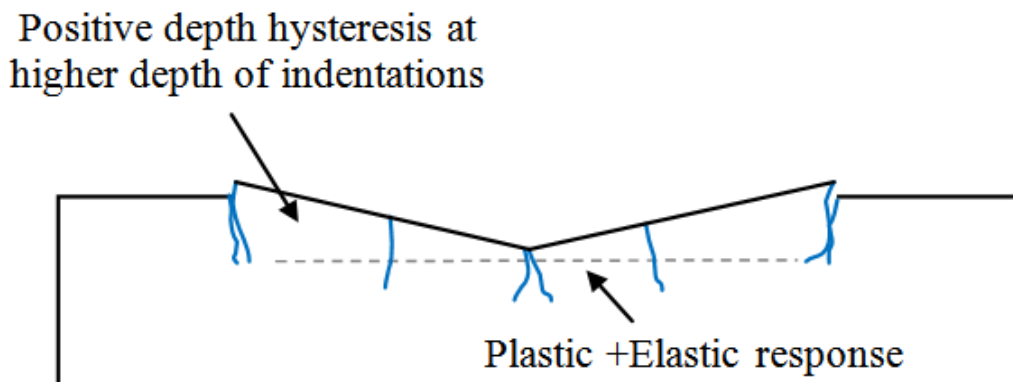
Figure 2(c) shows the P-h plot for the indentation made on 4H-SiC specimen at depth of 12 nm. Unlike the indents performed at depths of 2 nm and 5 nm, no depth hysteresis was observed in these plots. This implies that the material made a complete elastic recovery and unloading curve followed the same trend like that of the loading curve. Figures 2(d), 2(e) and 2(f) show the P-h plots for the indentation made on 4H-SiC specimen at depths of 25 nm, 30 nm and 50 nm respectively. In these figures, the indentation plot shows a different response of the specimen i.e. the ratio of h_f/h_{max} is less than unity and at an indentation depth of 50 nm a clear positive depth hysteresis is observed from these plots. As explained in the next section, this positive hysteresis is a result of the incipient plasticity in 4H-SiC. The typical response of the 4H-SiC specimen is schematically presented in figure 4, highlighting the behaviour of the specimen under different depth of indentations as has been explained above.



(a) Indentation in 4H-SiC at lower depths of upto 10 nm



(b) Indentation in 4H-SiC at depths 12 nm



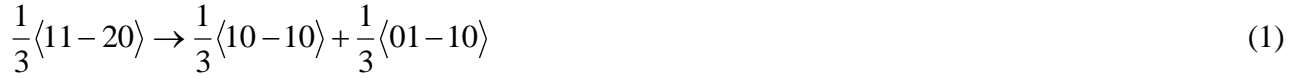
(c) Indentation in 4H-SiC at higher depths

Figure 4: Schematic of the depth hysteresis observed during nanoindentation of 4H-SiC

3.2. Incipient plasticity in 4H-SiC

Recently, grain boundary (g.b) analysis in conjunction with Large Angle Convergent Beam Electron Diffraction (LACBED) was used to propose that that dislocations in 4H-SiC were observed to be in

the basal plane with their Burgers vector as $\frac{1}{3}\langle -1-120 \rangle$ [36]. Also, perfect dislocations in 4H-SiC were proposed to dissociate into Shockley partials as per the following reaction:



For brittle materials like 4H-SiC, there may be two types of defect nucleations: dislocations or micro-cracks. The dislocations are induced by the onset plasticity, occurring when the maximum shear stress beneath the indenter exceeds the theoretical shear strength of 4H-SiC. Hertzian theory suggests that the maximum tensile stress is at the edge of the indenter. This stress acts in a radial direction on the surface outside the indenter, and is usually responsible for the cone cracks [37]. When the tensile strength does not exceed the value of theoretical cleavage strength or when the maximum shear stress below the indenter tip approaches the theoretical shear strength, then a pop-in event could occur due to the incipient plasticity. Ostensibly, the pop-in event (kink showed in figure 2f) arises from the nanomechanical response of the material, possibly due to an activity of defect nucleation underneath the indenter [31]. The parabolic shape of the P-h curve indicates elastic contact while displacement burst plus shallower slope is reminiscent of a combination of elastic and plastic response. Beyond this point, the unloading curve follows the power law curve.

An analytical stress analysis was carried out to find the state of stress underneath the indenter in order to reveal the minutiae of the pop-in event. Before the pop-in event, the P-h curve follows the Hertzian contact theory which could be expressed using the following equation:

$$P = \frac{4}{3} Er \sqrt{Rh^3} \quad (2)$$

where P is the indentation load, h is the displacement of the indenter, R is the radius of the indenter (300 nm) and Er is the reduced elastic modulus where Er can be expressed as:

$$\frac{1}{E_r} = \frac{1-\nu^2}{E} + \frac{1-\nu_i^2}{E_i} \quad (3)$$

In the above expression ν and E are the Poisson's ratio and elastic modulus of 4H-SiC [12] respectively while E_i and ν_i are the elastic modulus and Poisson's ratio of the diamond indenter

which were considered as 1141 GPa and 0.07 respectively. This gives the value of E_r as 296 GPa for the current combination of diamond and 4H-SiC.

In order to assert if the pop-in event in Figure 2(f) relates to the plastic deformation due to dislocation nucleation or crack propagation, an analysis is presented below. This analysis is based on evaluation of the maximum shear stress and maximum tensile strength underneath the indenter during the process of nanoindentation. The maximum shear stress underneath the indenter can be found out using the following equation [14]:

$$\tau = 0.47 \frac{P}{\pi.R.h} \quad (4)$$

This gives an estimate of τ (shear stress) as 21 GPa at an indentation depth of 33 nm at a typical indentation load ($P = 1500 \mu\text{N}$) where pop-in event was observed. To compare and correlate this shear stress with plastic deformation, the theoretical shear strength of 4H-SiC was obtained from the following equation [38]:

$$\text{Shear strength of 4H - SiC} = \frac{G}{2\pi} = \frac{131.4}{2\pi} = 20.9 \text{ GPa} \quad (5)$$

where G is the shear modulus and is experimentally known to be about 131.4 GPa for 4H-SiC.

It can be seen that the shear strength of 4H-SiC (20.9 GPa) corroborates well with the shear stress of 21 GPa estimated to be underneath the indenter during the pop-in event. This seems to suggest an occurrence of plastic deformation in 4H-SiC underneath the indenter. It is to be noted that plastic deformation can be affirmed if another criterion for plastic deformation is fulfilled i.e. the tensile stresses underneath the indenter need to be lower than the cleavage strength of 4H-SiC.

The tensile stresses and cleavage strength of 4H-SiC were obtained using the following equation [14]:

$$\sigma_{\max} = \left(\frac{1-2\nu}{2\pi} \right) \left(\frac{4E}{3R} \right)^{2/3} P^{1/3} \quad (6)$$

where σ_{\max} is the tensile strength underneath the indenter, P is the indentation load (1500 μN), ν is

the Poisson's ratio (0.23) of 4H-SiC, E is the elastic modulus (347 GPa) [12] of 4H-SiC and R is the indenter radius (300 nm).

Substitution of the experimental values in the above equation reveals the magnitude of tensile stress to be about 10.155 GPa underneath the indenter. For fracture or cleavage to dominate over plastic deformation, the cleavage strength of 4H-SiC must be lower than the value of this tensile stress. The following equation was used to calculate the cleavage strength of 4H-SiC.

$$\text{Cleavage strength of 4H - SiC} = \frac{1}{2} \sqrt{\frac{E\gamma}{a}} \quad (7)$$

where E is the elastic modulus of 4H-SiC (347 GPa), γ is surface tension (6.5 J/m² [39]) and a is the interplanar spacing (3.079 Å) in 4H-SiC.

Substitution of the above values reveals the magnitude of cleavage strength to be 13.53 GPa. Figure 5 shows the evolution of the tensile stress and shear stress underneath the indenter (the figure was drawn using equations (2), (3), (4), (5), (6) and (7)) and highlights the theoretical shear strength and theoretical cleavage strength of 4H-SiC.

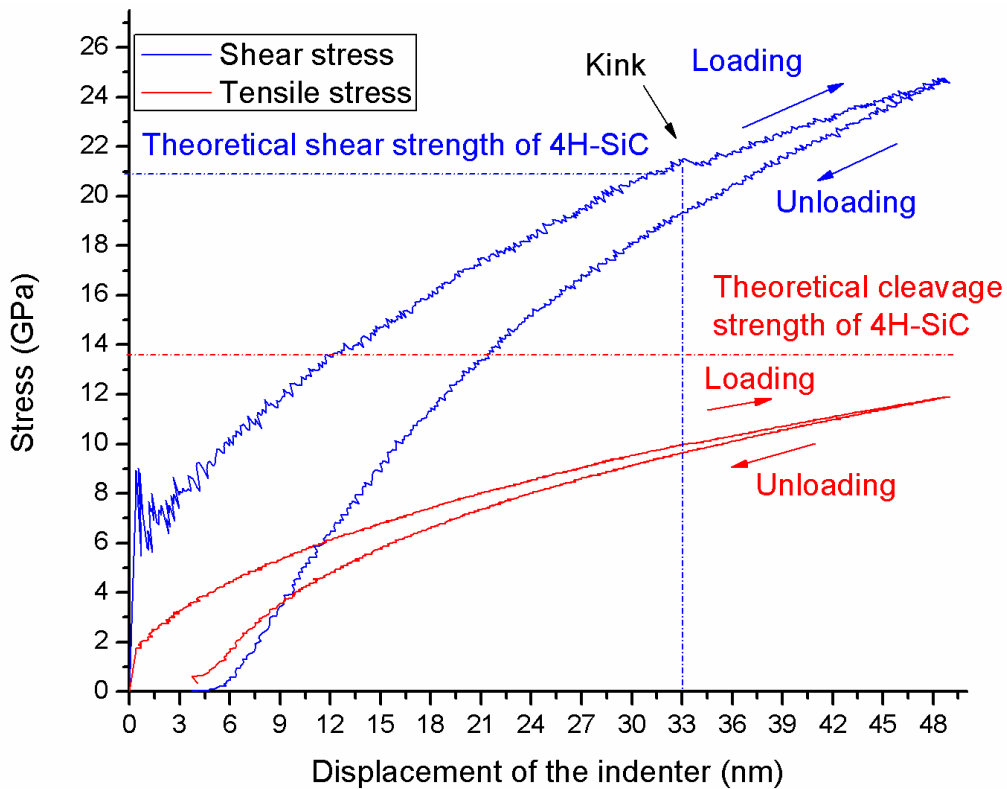


Figure 5: Evolution of shear stress and tensile stress underneath the Berkovich indenter (300 nm edge radius) during nanoindentation of nanocrystalline 4H-SiC at indentation depths up to 50 nm

It can be seen from Figure 5 and from the above calculations that the theoretical shear strength calculation coincides with the pop-in event observed at an indentation depth of 33 nm whereas the tensile stresses at this point were far lower (10.155 GPa). This proves that the plastic deformation in 4H-SiC during the pop-in event leads to cleavage and thus explains that the observed incipient plasticity is due to plastic deformation rather than the micro cleavage or fracture in 4H-SiC. The analysis presented above also reveals that during contact loading of single crystal 4H-SiC, tensile and shear stresses underneath the indenter increase with an increase in the indentation depth. At shallow depths of indentation (33 nm while using an indenter with the edge radius of 300 nm), the induced shear stress is lower than the theoretical shear strength of the specimen and hence material showed pure elastic response. With an increase in the extent of load, when the shear stress underneath the indenter exceeds the theoretical shear strength of 4H-SiC, a pop-in event is observed, which indicates induced plastic response. Such a plastic response is due to the plastic deformation and not because of the crack propagation because until this point, the theoretical cleavage strength is much higher than the tensile stress underneath the indenter.

4.0 Conclusions

Displacement controlled quasistatic nanoindentations on single crystal 4H-SiC were analyzed. Typically below a shear stress of 21 GPa, 4H-SiC showed purely elastic response while plasticity was observed beyond this point. Based on the foregoing discussions, following other conclusions can be drawn:

1. Three distinct patterns in the P-h plots were observed during nanoindentation of 4H-SiC (i) with negative depth hysteresis (ii) with no depth hysteresis and (iii) with positive depth hysteresis. This depth hysteresis is proposed to arise from compressive residual stresses (~143 MPa).

2. An analytical stress analysis was carried out to calculate the theoretical shear strength and cleavage strength of 4H-SiC along with the shear stress and tensile stress underneath the indenter. The theoretical shear strength was estimated to be about 20.9 GPa which was found to corroborate with the shear stress (21GPa) underneath the indenter whereas the theoretical cleavage strength was estimated to be 13.53 GPa which was noted to be much higher than the estimated tensile stress of 10.155 GPa underneath the indenter. Comparison of these values reveals that pop-in event occurred on account of plastic deformation in 4H-SiC rather than fracture (thus indicating that the pop-in event is an outcome of the incipient plasticity in 4H-SiC).

Acknowledgments:

Authors greatly acknowledge the funding support from J M Lessells travel scholarship from the Royal Society of Edinburgh (2013 RSE/J M Lessells Travel Scholarship) and an additional funding from the International Research Fellowship account of Queen's University, Belfast. Authors also greatly acknowledge an additional funding from an EPSRC research grant (Ref: EP/K018345/1).

References:

1. Neudeck, P.G., *SiC Technology*, in *The VLSI Handbook*, B. Raton, Editor. 2000, CRC Press and IEEE Press: Florida. p. 6.1-6.24.
2. Dzurak, A., *Quantum computing: Diamond and silicon converge*. *Nature*, 2011. **479**(7371): p. 47-48.
3. Shore, P., Cunningham, C., DeBra, D., Evans, C., Hough, J., Gilmozzi, R., Kunzmann, H., Morantz, P., and Tonnellier, X., *Precision engineering for astronomy and gravity science*. *CIRP Annals - Manufacturing Technology*, 2010. **59**(2): p. 694-716.
4. Newsome, D.A., Sengupta, D., Foroutan, H., Russo, M.F., and van Duin, A.C., *Oxidation of Silicon Carbide by O₂ and H₂O: A ReaxFF Reactive Molecular Dynamics Study, Part I*. *The Journal of Physical Chemistry C*, 2012. **116**(30): p. 16111-16121.
5. Coletti, C., Jaroszeski, M., Pallaoro, A., Hoff, A., Iannotta, S., and Sadow, S. *Biocompatibility and wettability of crystalline SiC and Si surfaces*. in *Engineering in Medicine and Biology Society, 2007. EMBS 2007. 29th Annual International Conference of the IEEE*. 2007: IEEE.
6. Li, X., Wang, X., Bondokov, R., Morris, J., An, Y.H., and Sudarshan, T.S., *Micro/nanoscale mechanical and tribological characterization of SiC for orthopedic applications*. *Journal of Biomedical Materials Research Part B: Applied Biomaterials*, 2005. **72B**(2): p. 353-361.
7. Coletti, C., Jaroszeski, M., Hoff, A.M., and Sadow, S.E. *Culture of mammalian cells on single crystal SiC substrates*. in *Mater. Res. Soc. Symp. Proc.* 2006: Cambridge Univ Press.
8. Kalnins, U., Erglis, A., Dinne, I., Kumsars, I., and Jegere, S., *Clinical outcomes of silicon carbide coated stents in patients with coronary artery disease*. *Medical science monitor: international medical journal of experimental and clinical research*, 2002. **8**(2): p. PI16-20.

9. Inasaki, I., *Grinding of Hard and Brittle Materials*. CIRP Annals - Manufacturing Technology, 1987. **36**(2): p. 463-471.
10. Komanduri, R., *On Material Removal Mechanisms in Finishing of Advanced Ceramics and Glasses*. CIRP Annals - Manufacturing Technology, 1996. **45**(1): p. 509-514.
11. Perrone, D., *PhD Thesis, Process and characterisation techniques on 4H - Silicon Carbide*, in *Micronanotechnology*. 2007, Politecnico di Torino: Torino.
12. Luo, X., Goel, S., and Reuben, R.L., *A quantitative assessment of nanometric machinability of major polytypes of single crystal silicon carbide*. Journal of the European Ceramic Society, 2012. **32**(12): p. 3423-3434.
13. Ravindra, D., Patten, J., and Jacobsen, R., *Hybrid laser ablation–single point diamond turning machining process for CVD–silicon carbide ceramics*. International Journal of Manufacturing Research, 2013. **8**(3): p. 227-249.
14. Zhao, X., Langford, R.M., Shapiro, I.P., and Xiao, P., *Onset Plastic Deformation and Cracking Behavior of Silicon Carbide under Contact Load at Room Temperature*. Journal of the American Ceramic Society, 2011. **94**(10): p. 3509-3514.
15. Patten, J., Gao, W., and Yasuto, K., *Ductile Regime Nanomachining of Single-Crystal Silicon Carbide*. Journal of Manufacturing Science and Engineering, 2005. **127**(3): p. 522-532.
16. Levitas, V.I., Ma, Y., Selvi, E., Wu, J., and Patten, J.A., *High-density amorphous phase of silicon carbide obtained under large plastic shear and high pressure*. Physical Review B, 2012. **85**(5): p. 054114.
17. Goel, S., Luo, X., Comley, P., Reuben, R.L., and Cox, A., *Brittle–ductile transition during diamond turning of single crystal silicon carbide*. International Journal of Machine Tools and Manufacture, 2013. **65**(February): p. 15-21.
18. Yan, J., Zhang, Z., and Kuriyagawa, T., *Mechanism for material removal in diamond turning of reaction-bonded silicon carbide*. International Journal of Machine Tools and Manufacture, 2009. **49**(5): p. 366-374.
19. Shayan, A.R., Poyraz, H.B., Ravindra, D., Ghantasala, M., and Patten, J.A., *Force Analysis, Mechanical Energy and Laser Heating Evaluation of Scratch Tests on Silicon Carbide (4H-SiC) in Micro-Laser Assisted Machining ([micro sign]-LAM) Process*. ASME Conference Proceedings, 2009. **2009**(43611): p. 827-832.
20. Ravindra, D. and J.A., P., *Determining the Ductile to Brittle Transition (DBT) of a Single-Crystal 4H-SiC Wafer by Performing Nanometric Cutting*, in *ISAAT 2007 Precision Grinding and Abrasive Technology at SME International Grinding Conference*. 2007.
21. Patten, J.A., Jacob, J., Bhattacharya, B., Andrew Grevstad, Ning Fang, and Marsh, E.R., *Chapter 2: Numerical simulations and cutting experiments on single point diamond machining of semiconductors and ceramics*, in *Semiconductor Machining at the Micro-Nano Scale*, ISBN : 978-81-7895-301-4, J. Yan and J.A. Patten, Editors. 2007, Transworld Research Network: Trivandrum-695 023, Kerala, India.
22. Bhattacharya, B., Patten, J.A., and Jacob, J., *Single Point Diamond Turning of CVD Coated Silicon Carbide*. ASME Conference Proceedings, 2006. **2006**(47624): p. 1153-1158.
23. Schuh, C.A. and Lund, A.C., *Application of nucleation theory to the rate dependence of incipient plasticity during nanoindentation*. Journal of Materials Research, 2004. **19**(07): p. 2152-2158.
24. V.C. Venkatesh and Sudin Izman, *Precision Engineering*, DOI: 10.1036/0071548270. 2007, New Delhi, India: Tata Macgraw Hill.
25. Chen, X., Hutchinson, J.W., and Evans, A.G., *The mechanics of indentation induced lateral cracking*. Journal of the American Ceramic Society, 2005. **88**(5): p. 1233-1238.
26. Ravindra, D., *Ductile mode material removal of ceramics and semiconductors*, in *Department of Mechanical and Aeronautical Engineering*. 2011, Western Michigan University: Michigan. p. 312.
27. Niihara, K., *Slip systems and plastic deformation of silicon carbide single crystals at high*

- temperatures. *Journal of the Less Common Metals*, 1979. **65**(1): p. 155-166.
28. *Probe Selection Guide - Hysitron Triboindenter Manual*, H. Incorporated, Editor. 2007: Minneapolis, USA.
 29. Javvaji, R., *Nanoscale ductile mode ultraprecision cutting of potassium dihydrogen phosphate*, in *Mechanical Engineering*. 2008, National University of Singapore: Singapore.
 30. Faisal, N., Ahmed, R., and Reuben, R., *Indentation testing and its acoustic emission response: applications and emerging trends*. *International Materials Reviews*, 2011. **56**(2): p. 98-142.
 31. Schuh, C.A., *Nanoindentation studies of materials*. *Materials Today*, 2006. **9**(5): p. 32-40.
 32. Kruzic, J.J., Kim, D.K., Koester, K.J., and Ritchie, R.O., *Indentation techniques for evaluating the fracture toughness of biomaterials and hard tissues*. *Journal of the Mechanical Behavior of Biomedical Materials*, 2009. **2**(4): p. 384-395.
 33. Feldman, D., Parker Jr, J.H., Choyke, W., and Patrick, L., *Phonon dispersion curves by Raman scattering in SiC, polytypes 3C, 4H, 6H, 15R, and 21R*. *Physical Review*, 1968. **173**(3): p. 787.
 34. Faisal, N.H., Ahmed, R., Fu, Y.Q., Elakwah, Y.O., and Alhoshan, M., *Influence of indenter shape on DLC film failure during multiple load cycle nanoindentation*. *Materials Science and Technology*, 2012. **28**(9-10): p. 1186-1197.
 35. Dharma Raju, T., Kato, M., and Nakasa, K., *Backward deviation and depth recovery of load-displacement curves of amorphous SiC film under repeating nanoindentation*. *Acta Materialia*, 2003. **51**(12): p. 3585-3595.
 36. Demenet, J.-L., Amer, M., Tromas, C., Eyidi, D., and Rabier, J., *Dislocations in 4H- and 3C-SiC single crystals in the brittle regime*. *physica status solidi (c)*, 2013. **10**(1): p. 64-67.
 37. Buzio, R., Boragno, C., Biscarini, F., De Mongeot, F.B., and Valbusa, U., *The contact mechanics of fractal surfaces*. *Nature Materials*, 2003. **2**(4): p. 233-236.
 38. Gouldstone, A., Koh, H.J., Zeng, K.Y., Giannakopoulos, A.E., and Suresh, S., *Discrete and continuous deformation during nanoindentation of thin films*. *Acta Materialia*, 2000. **48**(9): p. 2277-2295.
 39. Otubo, H., Yamamoto, Y., Takekuni, H., and Nishitani, S.R., *First principles calculations of relaxed and reconstructed surfaces of SiC*. Accessed through google.com on 26.8.2013.